

**Supplementary information:**

**Microwave-Assisted One-pot Synthesis of Anisotropic Gold Nanoparticles  
with Active High-Energy Facets for Enhanced Catalytic and Metal  
Enhanced Fluorescence Activities**

N. V. S. Praneeth and Santanu Paria\*

Interfaces and Nanomaterials Laboratory, Department of Chemical Engineering, National  
Institute of Technology, Rourkela-769008, Orissa, India

\*To whom correspondence should be addressed. E-mail: [sparia@nitrrkl.ac.in](mailto:sparia@nitrrkl.ac.in) or  
[santanuparia@yahoo.com](mailto:santanuparia@yahoo.com), Tel: +91 661 246 2262

## 1. Kinetics for the formation of Au NPs.

The total time taken for the completion of the reaction was studied using UV-Vis spectra at different time intervals at 30 °C and 50 °C on the hot-plate stirrer. The time when no further increment in the absorbance was observed considered as the reaction completion time.

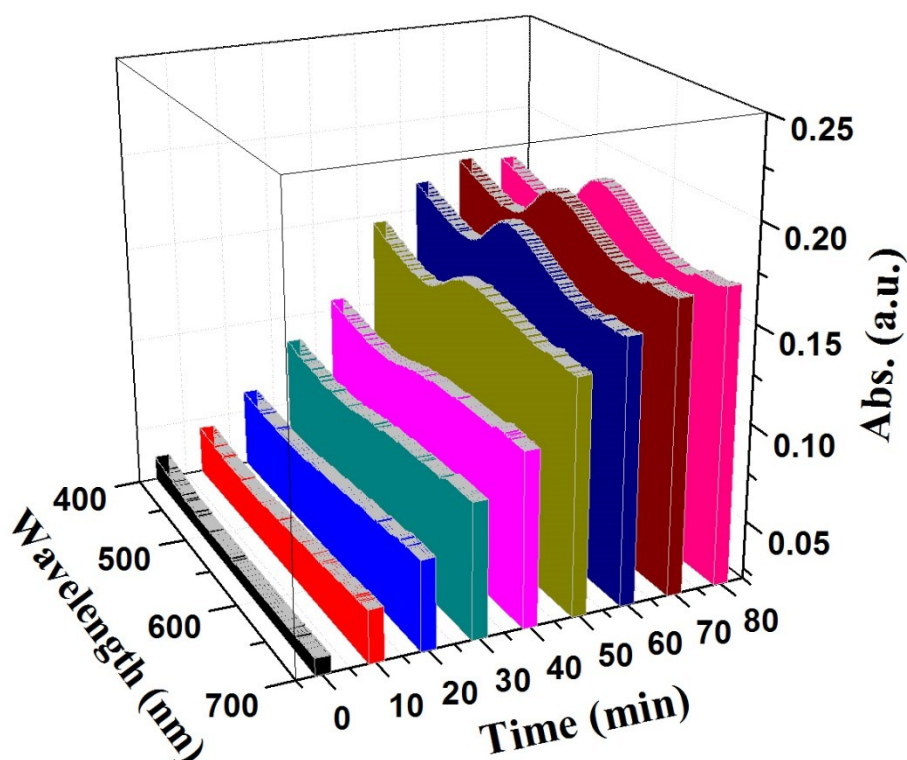


Figure S1a. Kinetic study (UV absorbance vs. time) for the formation of Au NPs at room temperature (30 °C).

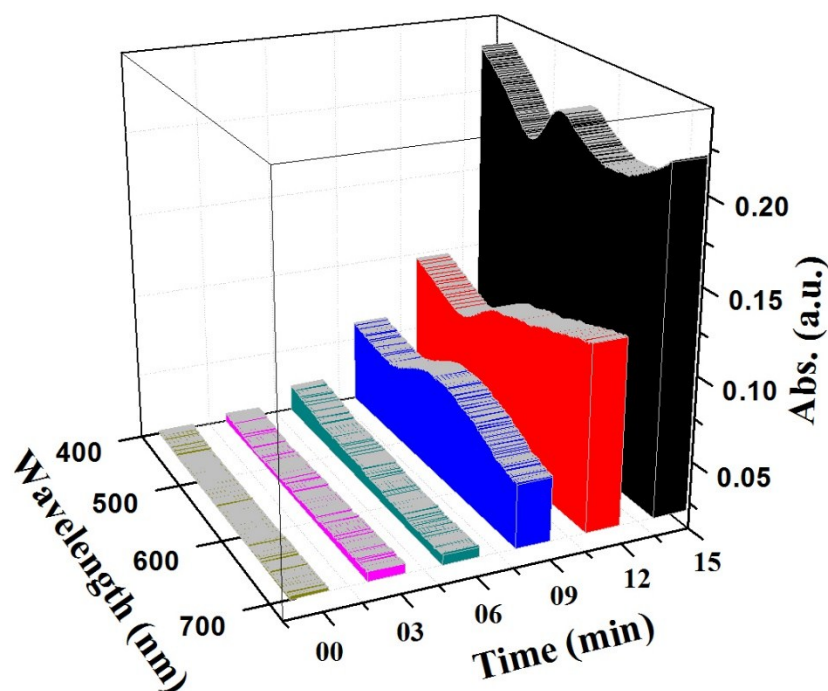


Figure S1b. Kinetic study (UV absorbance vs. time) for the formation of Au NPs at 50 °C.

## 2. Test for residual Gold precursor

All the studied ratios of  $[\text{Au}^{3+}]$ :  $[\text{OA}]$  were subjected to KBr test. The concentration of gold precursor was kept constant at 1mM for all the aforementioned ratios. The  $\text{KAuBr}$  complex forms a yellowish green precipitate and will have a distinct at 380 nm in UV-Vis spectroscopic analysis. The KBr was used in excess to fully react with the unreacted/excess Au precursor, therefore, the concentration of KBr was taken as 1 mM. 1mL of Au NPs suspension and KBr solution were mixed and stirred for 5 min then left as it is for an hour and then taken for UV-Vis spectroscopic analysis. The absence of any such colored precipitate and corresponding UV-Vis peak (Figure S2) for all the mentioned ratios confirms the complete reaction of Au precursor whereas we see a peak for in the presence of only  $\text{HAuCl}_4$ .

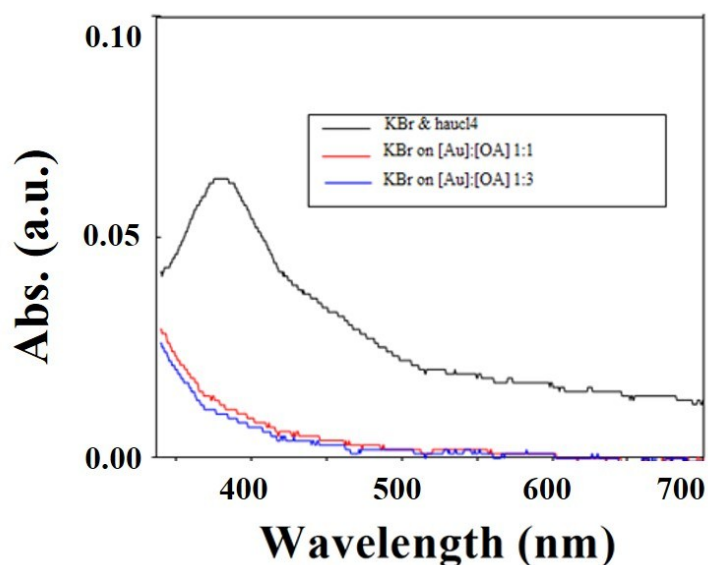


Figure S2. KBr analysis for residual Au precursor.

### 3. Hydrodynamic diameter study using Dynamic Light Scattering (DLS):

The hydrodynamic diameter of seeds is shown in the Figure S3, they were recorded by taking out the sample from the reaction mixture after given interval of time when the system was still in seed formation stage or before further growth in fully developed stable nanoparticles. The seed sizes were uniform distributed in the range 4-6 nm for MW conditions while for other RT and NMW condition the sizes were not so uniform at same time interval and ranged between 4-11 nm.

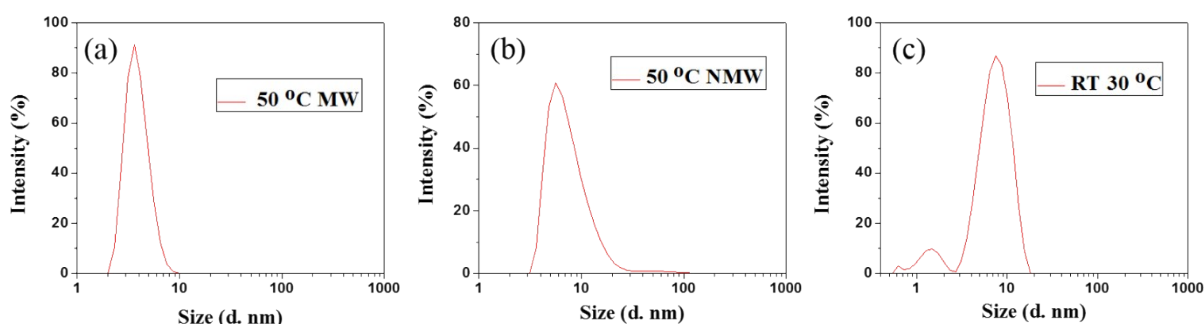


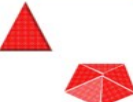
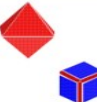








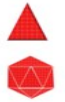

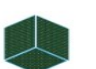

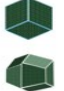







Figure S3. DLS size for seeds of 1:3 ratio at (a) MW ( $D_{avg} = 4.6$  nm), (b) NMW ( $D_{avg} = 7.4$  nm) at 50 °C and (c) RT ( $D_{avg} = 1.3$  nm,  $D_{avg} = 9.4$  nm) at 30 °C conditions.



### 4. The final shapes of the Au NPs



The effects of  $[OA]:[Au^{3+}]$  ratio, temperature, and heating type on the final shape of the nanoparticles in-situ growth after the seed formation was then studied. The formation of

different shapes under different conditions is schematically presented in Figure S4. Max. in the scheme depicts the shape of the majority of Au NPs and Min. depicts those shapes found in less number over a number of scanned regions in microscopic analysis.

Condition Reaction Ratio	RT		NMW		MW	
	Max	Min	Max	Min	Max	Min
1:1						
1:3						
1:5						
1:10						

 Sharp/Smooth icosahedron  
 2D Plates

 Decahedral  
 Octahedral

 Pseudo-spherical  
 Truncated-Cube/ cuboctahedron



 Squashed Dodecahedron  
 Rhombic Dodecahedron

Figure S4: Schematic representation of final shape with their external facets at different conditions along with their broad distribution in the system. {111}, {100} and {110} planes are shown in red, blue and green respectively and pseudo-spherical which has polycrystallinity is shown in yellow.

### 5. Growth mechanism of Au NPs formed at 1:1, 1:5 and 1:10 ratios of $[\text{Au}^{3+}]$ : $[\text{OA}]$ :

The Au NPs prepared at 1:1 ratio at different temperatures and heating methods are presented in Figure S5. The particles prepared at 30 °C are seen to be of irregular shape with spherical curvature or pseudo-spherical (Figure S5 a, b, c). The slow rate of reaction owing to weak reducing character of OA causes slow formation of  $\text{Au}^0$  as well as further growth. In general, initially formed twinned seed structures are known to grow into decahedron or icosahedron<sup>1</sup> NPs, however, in this case, the particles are having smooth spherical curvatures compared to sharper decahedron or icosahedron because of slow addition of  $\text{Au}^0$  which helps to minimize the surface energy. At 50 °C under NMW heating the presence of decahedron and icosahedron

structures are significant. Since the rate of reaction increases considerably at elevated temperature because of the higher kinetic energy of the molecules, nucleation and subsequent deposition of  $\text{Au}^0$  on the seed surface is spontaneous. As discussed earlier, there is a temperature induced a structural change of the seeds with the formation of some single-twinned and single crystalline structures. The addition of  $\text{Au}^0$  atoms on these transformed seeds and the interparticle growth along  $\{111\}$  facets, which are thermodynamically more favorable because of least surface energy of  $\{111\}$  among other low energy facets, and gives rise to the formation of plate and truncated octahedron Au NPs as shown in the SEM and TEM images of Figure S5 (d, e, f). Truncated octahedrons are because of faster addition of  $\text{Au}^0$  and stabilizing along  $\{100\}$  facet which gives the flat surface on edges called truncation.

In case of MW heating to the above condition, multi-twinned seeds were totally absent, as a result, the decahedral/icosahedral structures were also absent as shown in Figure S5 (g, h, i). Mostly single crystalline seeds were formed and allowed to grow octahedron/truncated-octahedron and cuboctahedrons bound by  $\{111\}$  and  $\{100\}$  facets. The cuboctahedrons bound by  $\{111\}$  and  $\{100\}$  facets are known to be most favorable equilibrium shape for the metals NPs of  $>20$  nm size because of minimum interfacial energy over other geometries <sup>45</sup>. In case of mixing ratios of 1:1 and 1:2 under both NMW and MW, no significant change in final structure was observed, a similar observation was for the mixing ratio of 1:3 and 1:4

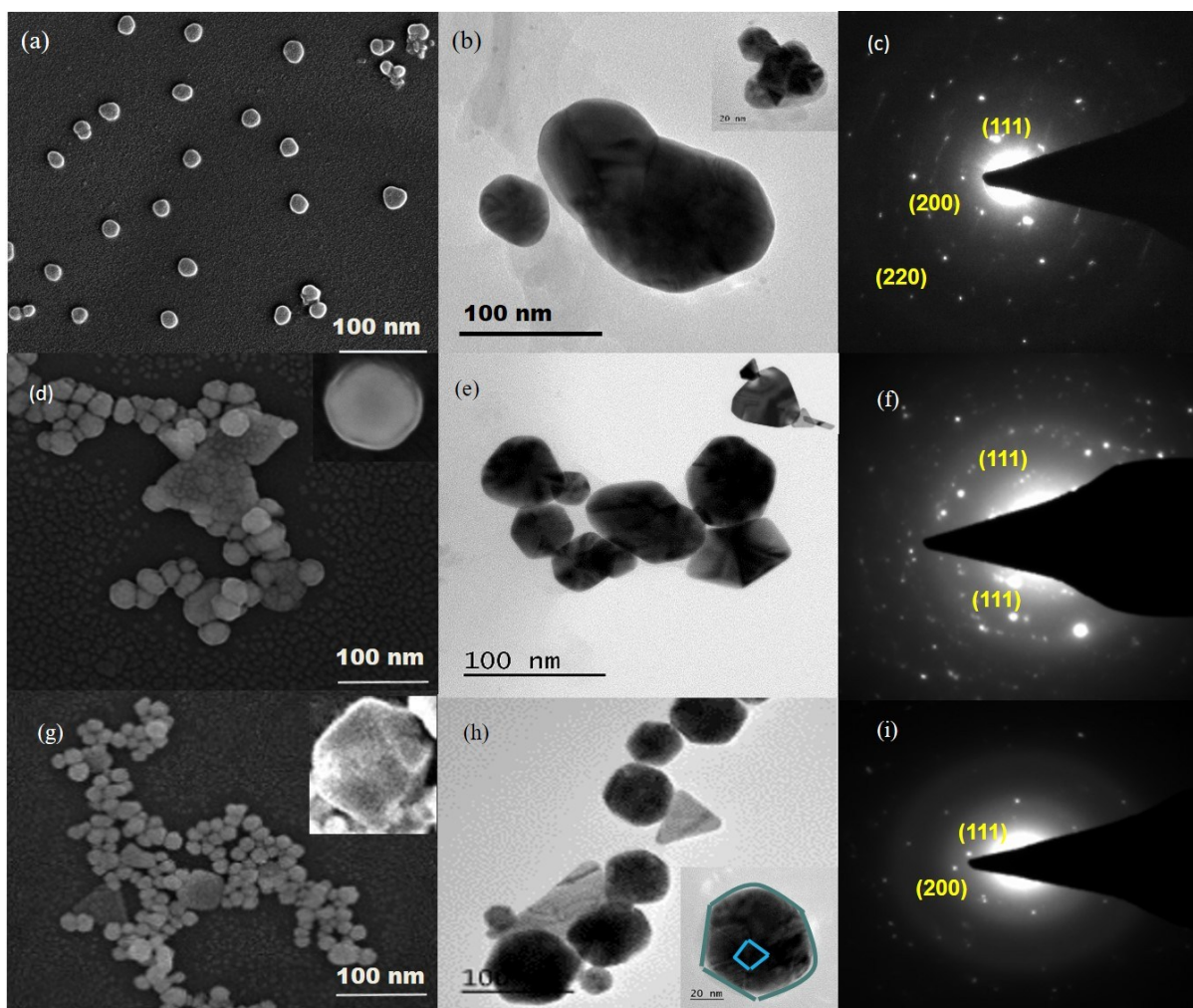


Figure S5. (a, b, c) FE-SEM, TEM, and SAED pattern of Au NPs prepared at 1:1 ratio at 30 °C. Inset shows the few decahedral nanoparticles fusing to form irregular shape and HR-TEM images showing the polycrystalline structure of these particles. (d, e, f) FE-SEM, TEM, and SAED pattern of Au NPs formed at 50 °C NMW. Inset shows magnified FE-SEM image of icosahedral shape. (g, h, i) FE-SEM, TEM, and SAED pattern of Au NPs formed at 50 °C MW. Insets are magnified images of octahedral Au NPs.

Au NPs prepared at higher ratios of 1:5 and above under all the studied conditions showed 2D plates of sub-micron size with characteristic dominant  $\{111\}$  facet (Figure S6) along with few twinned decahedrons and icosahedrons. In this case, the excess OA also acts as a capping agent by adsorbing on the  $\{111\}$  facet and finally resulting in plate type structures by allowing the growth along the lateral directions at the edges. Even at higher temperatures, OA capping prevents the formation of other shapes, hence the presence of plates is predominant at this ratio. The fast reduction rate due to high OA thus faster  $\text{Au}^0$  availability causes the size of Au NP to increase to sub-micron ranges. The SAED pattern of an isolated hexagon shows the presence



of forbidden  $1/3\{422\}$  plane, characteristic of plate type particles. Few icosahedrons and decahedrons were also present in this case, can be attributed to still insufficient OA concentration for complete capping of formed particles. However, this varied shape distribution was overcome when the ratio increased to 1:10, where the presence of only plate type structure was observed.

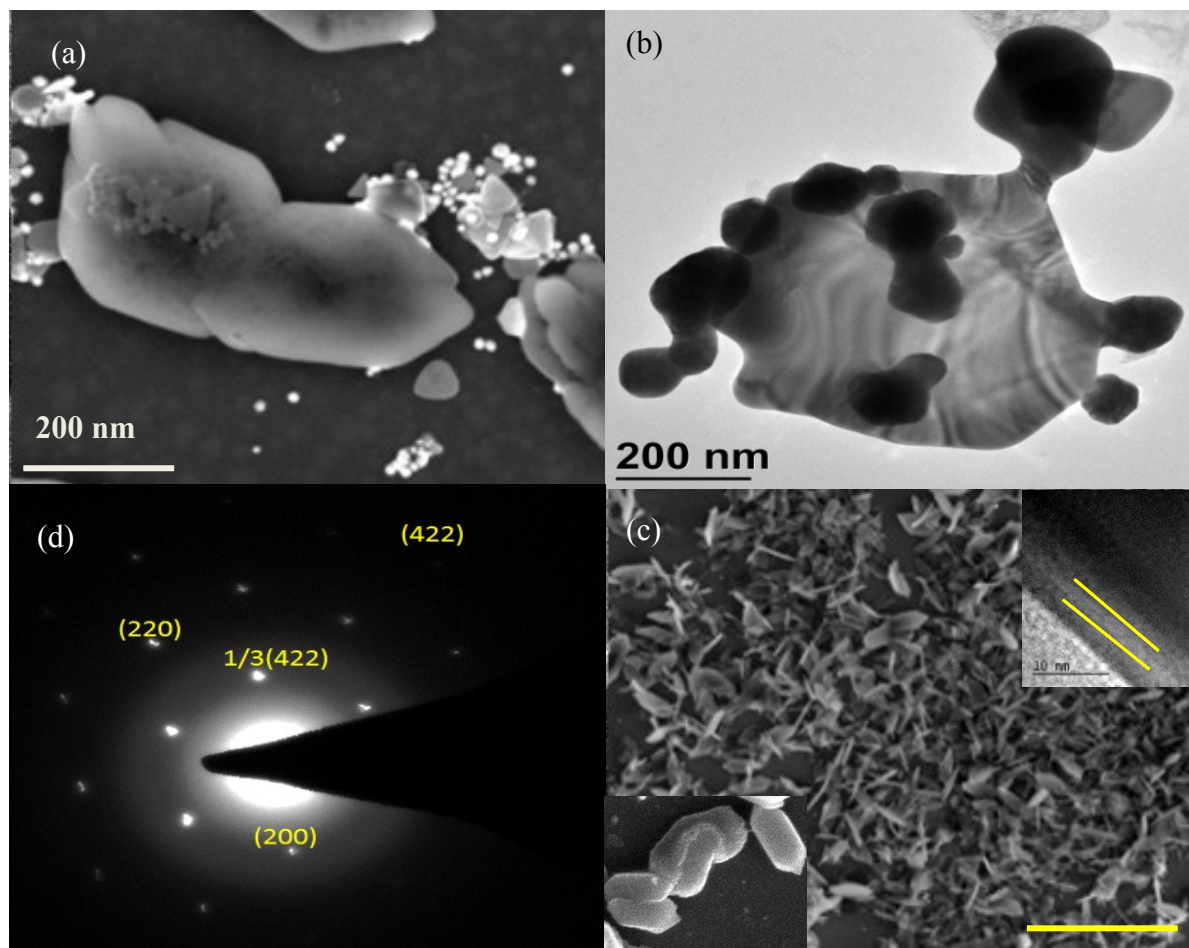


Figure S6. (a and b) FE-SEM and TEM image of Au NPs prepared at 1:5 ratio at 50 °C. (c) FE-SEM and HR-TEM image (inset) of Au NPs prepared at 1:10, yellow lines indicating stacking faults, scale bar 5  $\mu$ m (d) its corresponding SAED pattern.

#### 6. Size distribution of Au NPs formed at 1:3 ratios at different heating condition:

The size distribution of NPs formed at 1:3 ratios were observed using DLS and are shown in Figure S11. The hydrodynamic sizes are in agreement with that of the microscopically observed ones. The MW irradiated samples were of near about 50-70 nm so was the sample at 50 °C NMW whereas 30 °C prepared NPs were of wider size distribution as due to the formation of larger plate type NPs.



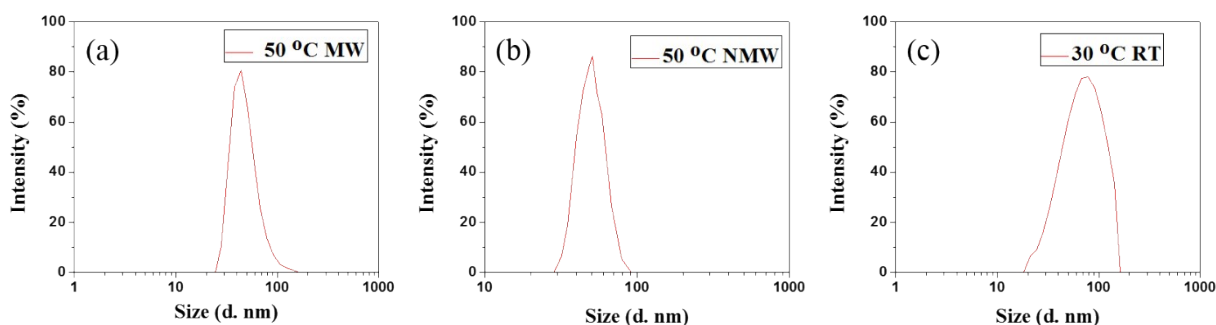


Figure S7. DLS size of Au NPs at 1:3 ratio under (a) MW ( $D_{\text{avg}} = 56.2$  nm), (b) NMW at 50 °C ( $D_{\text{avg}} = 59.1$  nm), and (c) RT at 30 °C ( $D_{\text{avg}} = 84.7$  nm).

## 7. XRD Analysis

The XRD diffractogram shown in Figure S7 supports the findings of crystallographic information of HR-TEM images and SAED patterns. The diffractogram for Au NPs prepared at 1:3 mixing ratio under non-MW heating shows the major peak of [111] facet at a diffraction angle ( $2\theta$ ) of  $36.5^\circ$ . The Au NPs prepared under MW irradiation show the presence of higher indexed facets of [200], [220] and [311] corresponding to diffraction angles of  $44.5^\circ$ ,  $65^\circ$ , and  $77.5^\circ$  respectively. The [220] reflection peaks become prominent in the MW heated method corresponding to formation of RD and QD along [110] plane, whereas in the non-MW method still has prominent [200] reflection peak which is attributed to higher formation of cuboctahedrons along with other structures. All these results are matched with JCPDS card No: 01-1174 and the formation of these crystalline facets were in line with findings of SAED analysis.

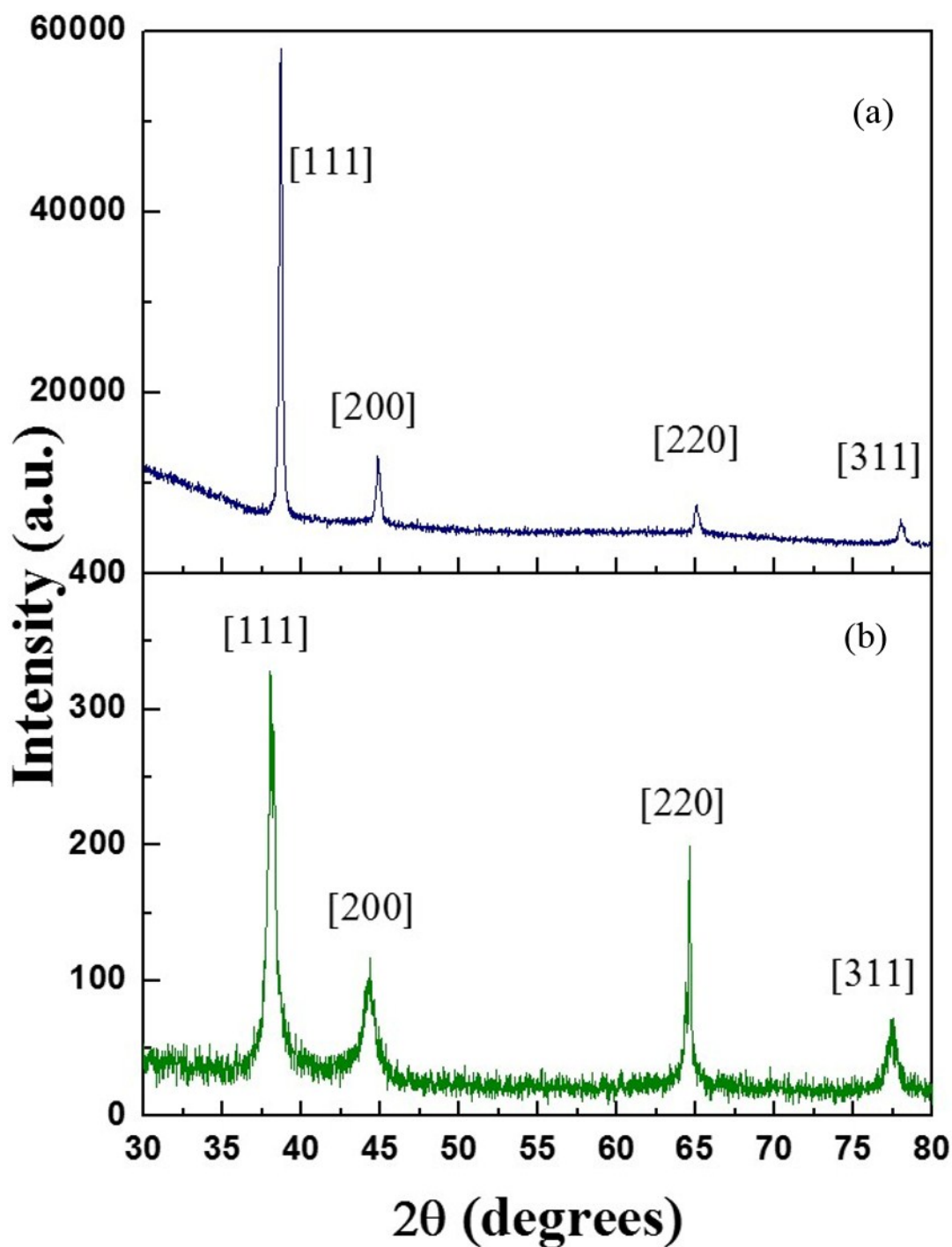


Figure S8. XRD of Au NPs from 1:3 ratios under (a) MW and (b) NMW heating.

### 8. Optical properties of Au NPs:

The Au NPs prepared at various mixing ratios exhibit different colors (Figure S9 and S10) mainly because of the variation of shapes and sizes, which are reflected in their SPR absorbance spectra as shown in Figure S8a. The particles prepared at 1:1 ratio shows the absorbance spectra similar to that of the mixed particles with a broad peak in the range of 500- 700 nm. However,

for the ratio of 1:3 spectra show a sharp peak at 540nm. The Au NPs prepared at 1:5 ratio shows an increase in absorbance in NIR region which can be attributed to the presence of plate type structures. The absorbance peak of the sample prepared at 1:5 ratio under both MW and NMW heating is similar, except the MW irradiated sample have a higher absorbance in NIR region (Figure S8b). The Au NPs prepared at higher  $[\text{Au}^{3+}]$ :  $[\text{OA}]$  ratio of 1:5 show an increased absorbance in NIR region which are typical of sub-micron 2D plate type structures previously reported.

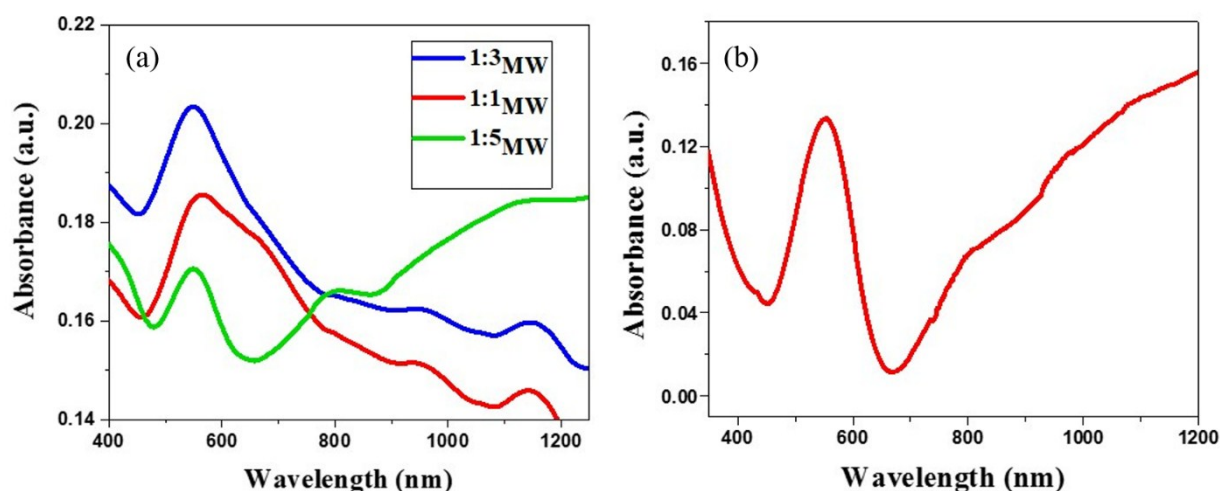


Figure S9. (a) UV-Vis-NIR spectra of Au NPs prepared from 1:1, 1:3 and 1:5 mixing ratios at 50 °C with MW heating. (b) UV-Vis-NIR spectra of Au NPs prepared at  $[\text{Au}]$ :  $[\text{OA}]$  of 1:5.

The variation in SPR spectra of anisotropic Au NPs compared to that of spherical can be attributed to the fact that the surface charges are more at edges and corners of the particles. The charge separation is higher in case of corners, this, in turn, reduces the restoring force for oscillation of electrons and causing a red shift in SPR absorbance. The broadening of peak of Au NPs prepared at higher ratio is attributed to variation in size and shape of the particles which causes the polarization at different wavelengths.

## 9. Color of Au NPs Suspension.

The Au NPs formed with ratios of 1:1, 1:2 and 1:3 under microwave condition were of different in color corresponding to their spectral absorbance and are shown in Figure S9 below.



Figure S10. Au NPs prepared at 1:5, 1:3 and 1:1 under MWH in that order from left to right.

The Au NPs prepared under conventional heating are shown in the Figure S10 with the temperature probe and the setup used for the reaction.

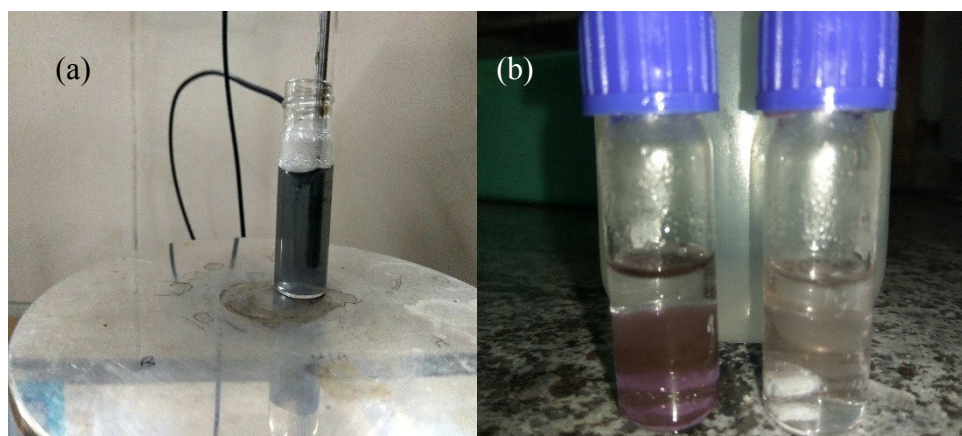


Figure S11. Au NPs prepared at 50 °C under conventional heating (NMW) (a) 1:5 and (b) 1:3 and 1:1, left to right respectively.

#### 10. 4-Nitrophenol reduction mechanism:

The atomic arrangement of dominant crystal facets exposed at the surface of Au NPs prepared under different MW heating at different ratios are shown in Figure S12. It can be visibly understood that the available surface atoms for adsorption of reactants are highest for {110} and least for {111} facet, with even inner atomic plane accessible for molecule adsorption in {110} faceted surface.

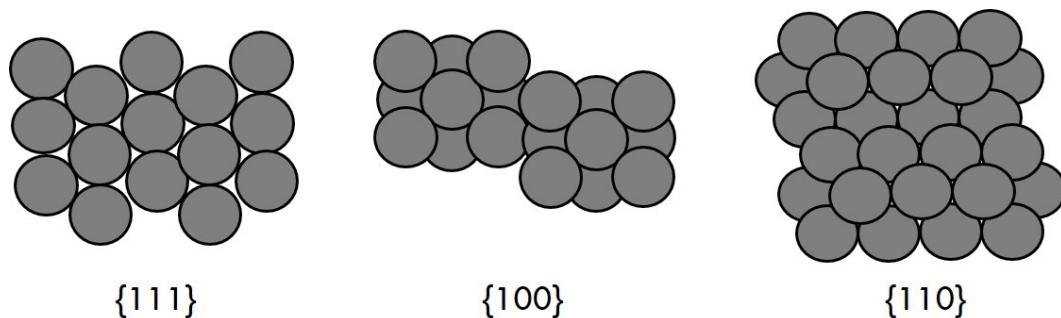
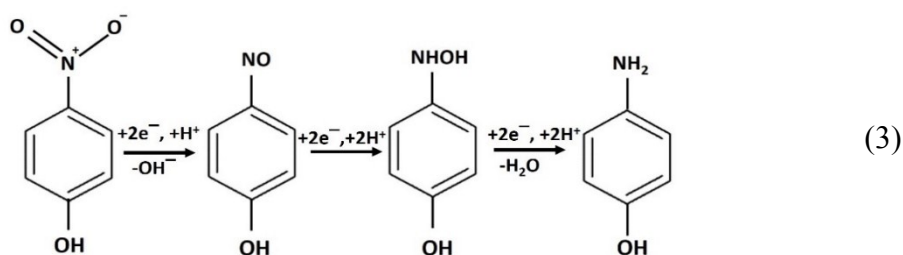


Figure S12. The arrangement of Au atoms across different facets.

In the aqueous solution,  $\text{NaBH}_4$  hydrolyses to  $\text{NaB(OH)}_4$  and releasing  $\text{H}^+$  and 8 electrons, the Au NPs accept these electrons and form Au-H bond with the surface atoms which then react with the adsorbed 4-NPh. The reduction process involves 6 electrons (Equations 1, 2) and proceeds with the formation of a 4-nitrosophenol intermediate with simultaneous condensation, finally forming 4-APh as shown in equation (3) which then desorbs from the surface. As adsorption and desorption processes are very fast, the rate determining step is the surface reaction, therefore the reaction rate increases with higher surface atoms.



## 11. Zeta-potential analysis:

The figure below shows the obtained zeta potential values of -18.9 and 44 mV before and after the addition of CTAB as a spacer to the Au NPs.

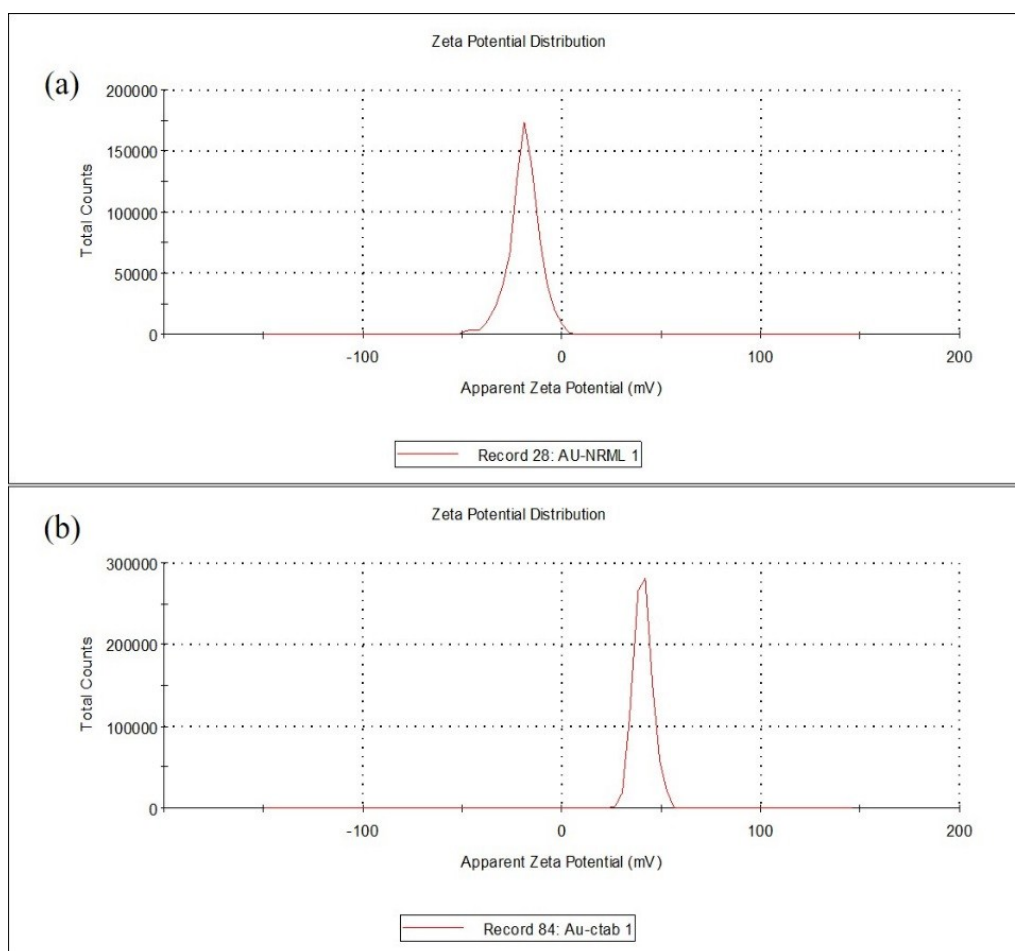


Figure S13. The zeta-potential plot of Au NPs (a) before and (b) after addition of CTAB.

## 12. DPBF degradation Spectra:

The UV-Vis absorbance spectra for degradation of DPBF, corresponding to  $^1\text{O}_2$  generation for 1:1<sub>MW</sub> and 1:3<sub>MW</sub> prepared Au NP-CTAB-RB conjugate is given in Figure S14.

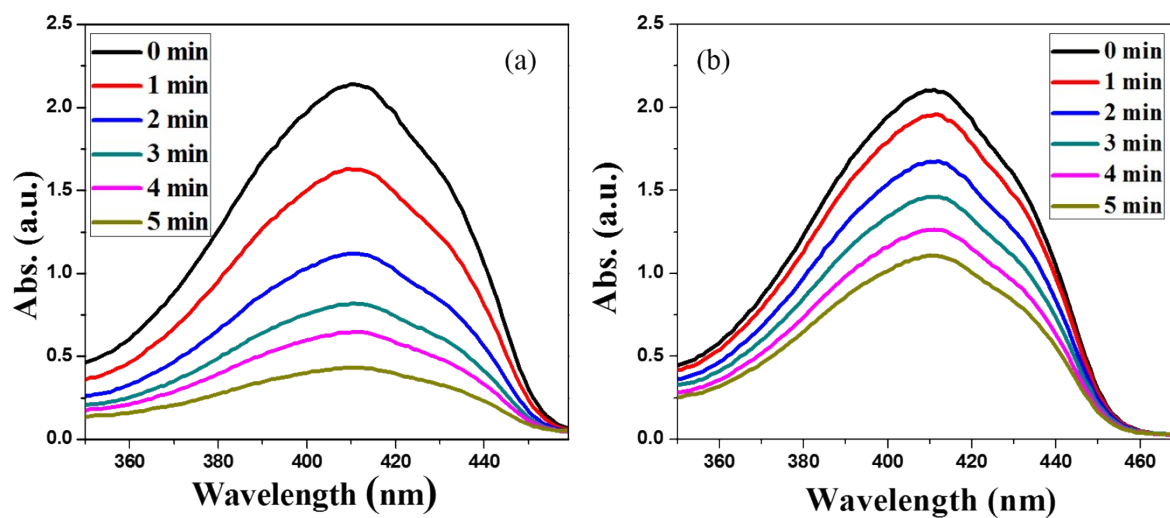




Figure S14. UV-Vis absorption spectra during DPBF degradation for (a) 1:3<sub>MW</sub> and (b) 1:1<sub>MW</sub> prepared Au NPs.

**Reference:**

- (1) Seo, D.; Yoo, C. Il; Chung, I. S.; Park, S. M.; Ryu, S. Shape Adjustment between Multiply Twinned and Single-Crystalline Polyhedral Gold Nanocrystals : Decahedra, Icosahedra, and Truncated Tetrahedra. *J. Phys. Chem. C* 2008, **112**, 2469–2475.